

ANL/ASD/CP--88210

CONF-9509227--13

RECEIVED

JAN 25 1995

OSTI

## Time-Domain Diagnostics in the Picosecond Regime\*

by

Alex H. Lumpkin  
Advanced Photon Source  
ASD/Diagnostics  
Argonne National Laboratory  
9700 S. Cass Ave.  
Argonne, IL 60439

### DISCLAIMER

This report was prepared as an account of work sponsored by an agency of the United States Government. Neither the United States Government nor any agency thereof, nor any of their employees, makes any warranty, express or implied, or assumes any legal liability or responsibility for the accuracy, completeness, or usefulness of any information, apparatus, product, or process disclosed, or represents that its use would not infringe privately owned rights. Reference herein to any specific commercial product, process, or service by trade name, trademark, manufacturer, or otherwise does not necessarily constitute or imply its endorsement, recommendation, or favoring by the United States Government or any agency thereof. The views and opinions of authors expressed herein do not necessarily state or reflect those of the United States Government or any agency thereof.

\*Work supported by the U.S. Department of Energy, Office of Basic Energy Sciences, under Contract No. W-31-109-ENG-38.

The submitted manuscript has been authored by a contractor of the U. S. Government under contract No. W-31-109-ENG-38. Accordingly, the U. S. Government retains a nonexclusive, royalty-free license to publish or reproduce the published form of this contribution, or allow others to do so, for U. S. Government purposes.

DISTRIBUTION OF THIS DOCUMENT IS UNLIMITED

MASTER

# Time-Domain Diagnostics in the Picosecond Regime\*

Alex H. Lumpkin

*Advanced Photon Source, ASD/Diagnostics, Argonne National Laboratory,  
9700 S. Cass Ave., Argonne, IL 60439, USA*

**Abstract.** The measurement of bunch length and longitudinal profile for microbunches of electrons and positrons in the ps and sub-ps regime will be a critical part of validating performance of proposed facilities. Data will be presented showing single-sweep streak camera results at  $\sigma_{\text{res}} \sim 68$  fs and projected synchroscan sweep resolution at  $\sigma \sim 600$  fs. Additionally, an rf cavity operating in a transverse magnetic mode has recently been shown to produce  $\sigma_{\text{res}} \sim 280$  fs when used with a low-emittance beam. The potential for dual-sweep streak work with  $\sigma_{\text{res}} < 1$  ps on the fast axis is also described.

## INTRODUCTION

The success of proposed applications of short bunches of electrons and positrons in linacs and storage rings will depend strongly on the ability to measure the microbunches bunch length and shape and to optimize appropriate parameters. The "streak camera principle" whereby a spatial dimension is transferred to a time dimension via a time-varying deflection of a beam is "alive and well" in 1995. This deflected "beam" can either be the accelerated beam or the photoelectron beam generated from the photocathode of a streak camera (1-3). Recently, camera systems have become commercially available that offer one-sigma resolution of about 85 fs or 200 fs (FWHM) (4). Even an old L-band rf deflector cavity at Los Alamos National Laboratory (5,6) has been used with a low emittance, 8-MeV beam to provide resolution of about 650 fs (FWHM). For the purposes of this workshop, this paper will address such time-domain diagnostics which give direct measures of bunch longitudinal profiles. It will also be assumed that the  $\text{FWHM} = 2.35\sigma$ . A number of other papers at this workshop will be addressing frequency domain work and the use of coherent transition radiation and coherent synchrotron radiation.

---

\*Work supported by the U.S. Department of Energy, Office of Basic Energy Sciences, under Contract No. W-31-109-ENG-38.

Additionally, I will consider the concept and use of dual-sweep streak cameras where the fast axis has  $\sim 600$  fs ( $\sigma$ ) resolution. These might be used to study dynamics of microbunches in a pulse train or circulating in a ring. The issue of on-line and off-line diagnostic capabilities will also be noted, as will the question of whether one wants to measure directly the output photon beams in some of the foreseen applications.

## EXPERIMENTAL BACKGROUND

As described in earlier papers (1-3), the streak principle uses the time-varying deflection of the electron beam in one spatial direction to convert this axis into a time axis. The time resolution and time coverage are dependent on beam spot sizes, deflection rates, and the physical space available.

### Beamline Streak (rf Deflector)

The case of the "beamline streak" using an rf deflector cavity is shown schematically in Fig. 1. This was positioned at the end of the beamline and after the

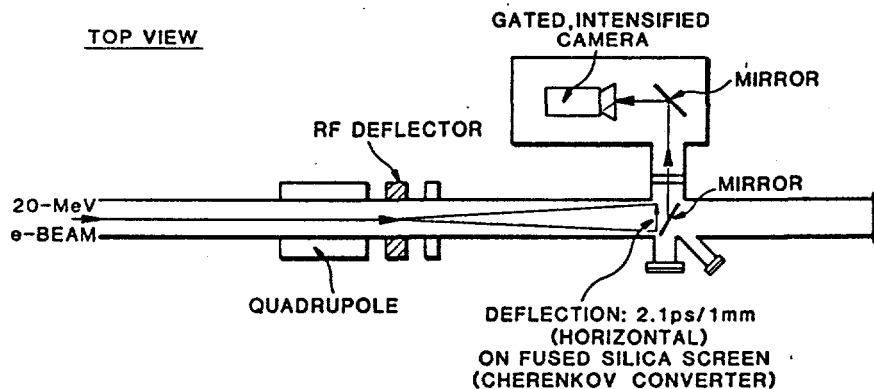


**FIGURE 1.** Schematic of a beamline streak system using the rf cavity, a converter screen, and a viewing camera.

wiggler in an early configuration of the Los Alamos FEL. The rf cavity (see Fig. 2) was developed by Stein (5) using an L-band cavity (1300 MHz) running in the transverse magnetic mode ( $TM_{110}$ ) to provide deflections of the 20-MeV electron beam of about 2.1 ps/mm at a distance of about 1 meter. It used 1 MW of rf power to the cavity. In another configuration, it was used with the spectrometer focal plane about 1 m away to provide energy information within the micropulse as well as the

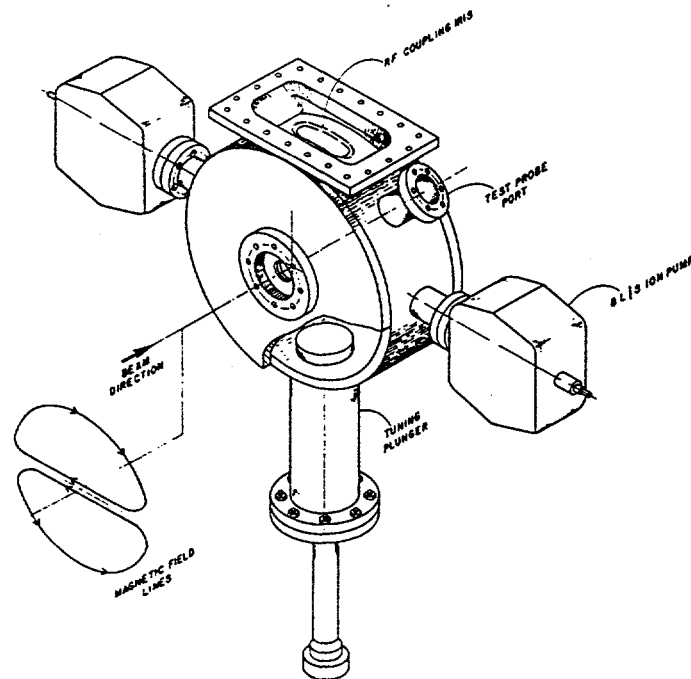


**FIGURE 2.** Schematic of a fast-deflector cavity and the orientation of the desired magnetic field in the cavity (from Ref. 5).

bunch length. In part due to the emittance of the thermionic gun used in those years, the beam spot was focusable to about 1 mm (FWHM) as measured on a 1/4-mm-thick fused silica screen oriented normal to the beam. The Cherenkov radiation was directed 90° to the beam by a polished metal mirror at 45° behind it. Needless to say, this was also a source of OTR, but in fact it was about 5 times weaker than the Cherenkov source. A gated, intensified camera provided the sensitivity and time-gate to select a single microbunch out of the 2000 micropulses and to measure its shape. For a low emittance beam, the OTR foil by itself is used to provide sub-100  $\mu\text{m}$  resolution. Actually, in the Los Alamos FEL program, both slow (macropulse 100  $\mu\text{s}$ ) and fast (micropulse  $\sim 10$  ps) deflection schemes on the beamline were used (1).

## Streak Cameras

Historically, the single-sweep streak cameras have had better time resolutions (2 ps (FWHM)) but more time jitter ( $\sim 10$  ps) than rf-synchronized or synchroscan units. A schematic of such a camera is shown in Fig. 3. The defining slit, the photocathode, the accelerating mesh, the deflection plates, the microchannel plate intensifier, and the output phosphor screen are indicated. The photoelectrons released at the photocathode are deflected vertically as a function of arrival time.

### PRINCIPLE OF OPERATION OF A STREAK CAMERA

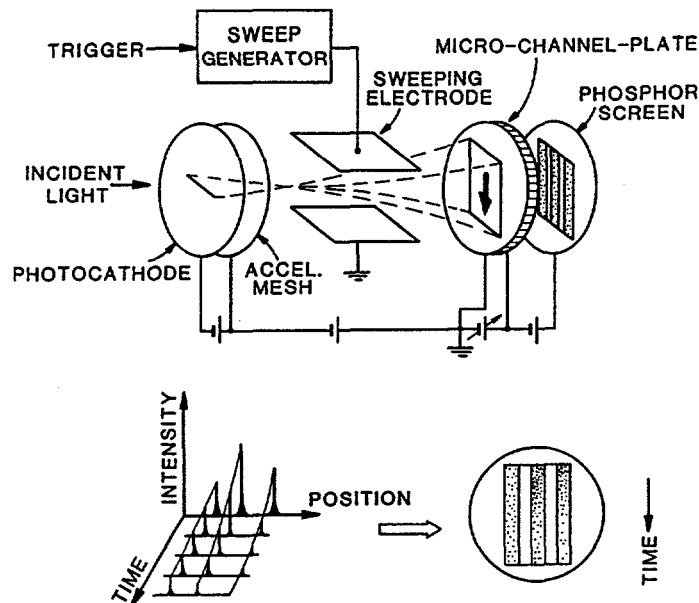


**FIGURE 3.** Schematic of a single-sweep streak camera tube showing the entrance slit, photocathode, deflection plates, microchannel plate intensifier, and phosphor.

This results in a "streak" of information on the output phosphor that can be recorded by film or camera. A video camera (intensified or of low noise) is a convenient solution to provide on-line information about the bunch length. With standard image processing techniques, the bunch length (FWHM) or  $\sigma$  can be calculated at a few Hz. As stated earlier, present single sweep streak cameras such as the Hamamatsu FESCA-200 report about 68 fs ( $\sigma$ ) resolution (4).

It has been my experience that for any application that involved an rf accelerator, the use of the synchroscan unit phase-locked to the master oscillator or some subharmonic paid significant dividends for dealing with bunch lengths less than 15 ps (FWHM). In the 1980's a trade was made in time resolution since such systems first had about 10 ps (FWHM) resolution with 4 ps jitter. Later models had 3 ps (FWHM) resolution with  $\sim 2$  ps jitter. Present models have about  $\sigma_{\text{res}} \sim 600$  fs and jitter reported as less than the resolution. Not only synchroscan, but also dual-sweep features are available. A second set of deflection plates orthogonal to the first set allows ps-phenomena to be tracked over pulse trains or turns in a ring. Examples on the linac-driven FEL and PEI drive laser application are well documented (2). The present examples will be based on phenomena observed on the rings of APS. The actual bunch length is much longer than 1 ps, but these data illustrate the concept graphically.

The actual bunch length ( $\Delta t_b$ ) is obtained by removing the camera resolution contribution in quadrature from the total observed bunch length ( $\Delta t_{\text{obs}}$ ).

Equation 1 includes the three contributions to the camera resolution

$$\Delta t_b^2 = \Delta t_{obs}^2 - [(\Delta t_1)^2 + (\Delta t_2)^2 + (\Delta t_3)^2] \quad (1)$$

where  $\Delta t_1$  is due to the energy distribution of secondary electrons and the photocathode uniformity,

$\Delta t_2$  is due to non-uniform electric potential at the deflection plates,

$\Delta t_3$  is due to the line spread function and the deflection speed.

The first term is estimated at  $\sim 1/2$  ps (FWHM) in the UV regime, but its contribution increases in the few angstrom regime.

## Calibration

The reliable calibration of these time measurements can be performed in a straightforward manner if the appropriate equipment is available. For the rf cavity deflector, the beam image size is recorded with the deflector power off, and then the minimum beam spot size is determined. With the deflector on, the variation of the phase for delivered rf power with the beam arrival time allows one to map out the effective degrees/mm or ps/pixel. A special quadrupole might be used to minimize the beam spot size in the deflection direction (5).

In a similar manner in the streak camera, the focus mode option allows one to determine the limiting spot size (static or line spread function) on the time axis. An optical etalon is used to generate a "train" of light pulses from the initial fast pulse with known time separations. These multiple images give a direct verification of deflection rate and linearity. A final test with a laser pulse of about 50 to 100 fs verifies the delivered resolution. For a synchroscan camera, a standard rf phase shifter can be placed in series with the rf oscillator input signal, the relative phase varied, and image locations logged. This method should agree with the etalon technique within a few percent.

## Conversion Mechanisms

If imaging techniques are to be used, the particle beam parameter information must be converted into optical (generally UV or visible) radiation that can be detected by the electro-optic devices. The conversion mechanism must be prompt compared to the bunch length involved. Mechanisms that have been employed are optical transition radiation (OTR), Cherenkov radiation (CR), spontaneous emission radiation (SER), optical synchrotron radiation (OSR), and the free-electron laser (FEL). The Smith-Purcell effect radiation (SPR) has perhaps a chance to become useful. Additionally, it should be noted that the photoelectric injector (PEI) is driven

by a drive laser whose wavelengths generally fall in the 0.25- to 1.05- $\mu\text{m}$  regime. These wavelengths are also directly addressable with a streak camera (2).

Another aspect to consider is whether the measurement technique is intercepting or nonintercepting to the beam. This has an immediate concern for the storage ring applications since the intercepting screens of Cherenkov and transition radiation are generally precluded. In fact, for low-emittance particle beams even in the linac, one probably could not leave the diagnostic foil inserted during the run in many cases. This is where the nonintercepting techniques based on OSR, SER, or SPR would have a potential advantage.

The efficiency of the conversion mechanism is also a consideration. Once one leaves the relatively intense/efficient world of fluorescence screens with their  $\sim 1$  ns or slower response times, the photon yield per particle ( $e^-$ ,  $e^+$ ) is somewhat comparable. The peaking of OTR into the  $1/\gamma$  cone angles makes it competitive with Cherenkov sources at the 50- to 100-MeV point. Even most linac beamlines have at least one bending magnet so the chance to use OSR should be considered. At Los Alamos we had imaged linac beams with energies as low as 22 MeV ( $\gamma=44$ ) (7). At facilities around the world, OSR has been used with beam energies up to 26 GeV at least.

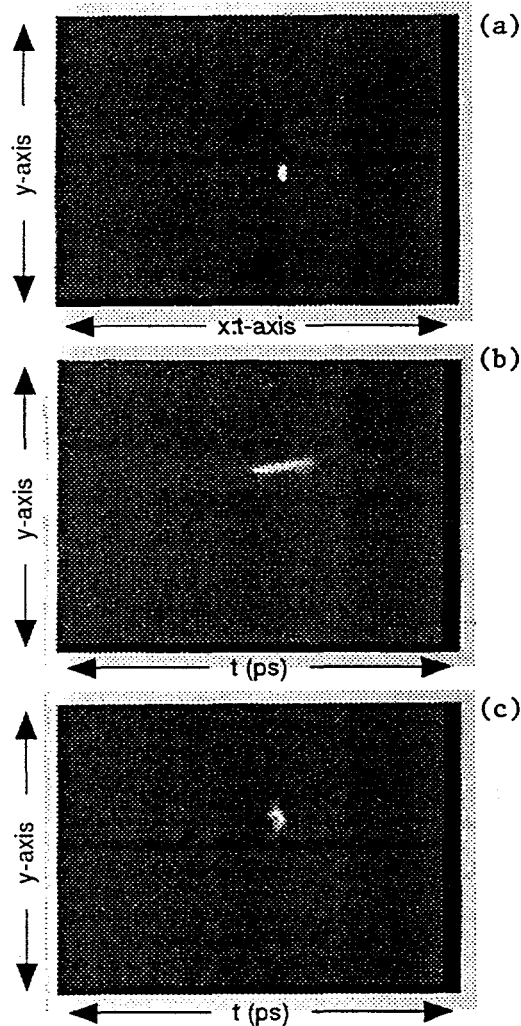
## Measurement Bandwidth

The measurement technique ideally should process its information in real-time mode, on-line mode, off-line mode, and off-line extended mode. Except for feedback issues, the human interface is part of the ergonomics of course. A human operator can see and process information in a few Hz, but probably would adjust parameters at 0.2 Hz. Visual display of results is readily done through the use of current imaging technologies. A video monitor display at 30 Hz for semi-quantitative results is real-time to an operator. A processing package that calculates bunch length at about a few Hz is reasonably on-line. A process that takes 10-30 minutes probably falls into semi-on-line, and processing times longer than 10s of minutes should probably be considered as off-line.

## EXAMPLES OF BUNCH LENGTH MEASUREMENTS

In this section some examples of time-domain measurements will be provided that show either subpicosecond resolution performance or a dual-sweep result that could be done with subpicosecond ( $\sigma$ ) resolution on the fast time axis with the appropriate source.

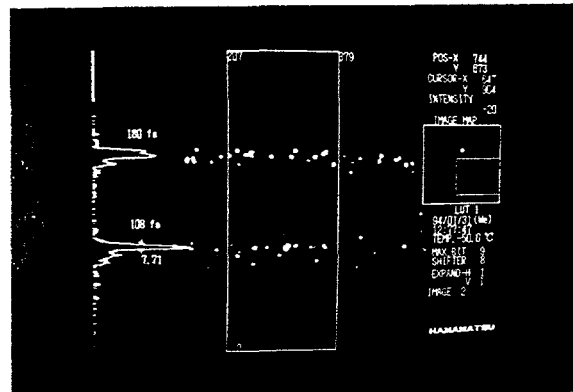
The first case addresses the beamline streak technique using the rf cavity performed at Los Alamos by Carlsten, et al. (6). The limiting resolution (deflector off) as shown in Fig. 4 is about 0.65 ps (FWHM) or 0.28 ps ( $\sigma_{\text{est}}$ ). This is illustrated



**FIGURE 4.** Recent results from the Los Alamos beamline deflection cavity and viewing system. Images show fast deflector off (a), fast deflector on plus phasing cavity at 12 MV/m (b), and phasing cavity on at 26 MV/m (c).

in Fig. 4a. The next two images show measurements (deflector on) of the bunch length with the injector phasing cavity at 12 MV/m (4b) and 26 MV/m (4c). The time/deflector axis is horizontal, and the reduction from 4.8 ps (FWHM) to 0.9 ps (FWHM) is directly observable. In addition, the vertical axis contains information about the y-profile and position during the microbunch. The small y-t tilt exhibited in Fig. 4b illustrates the signature of a head-tail effect, but any image/deflector alignment tilt must first be subtracted.

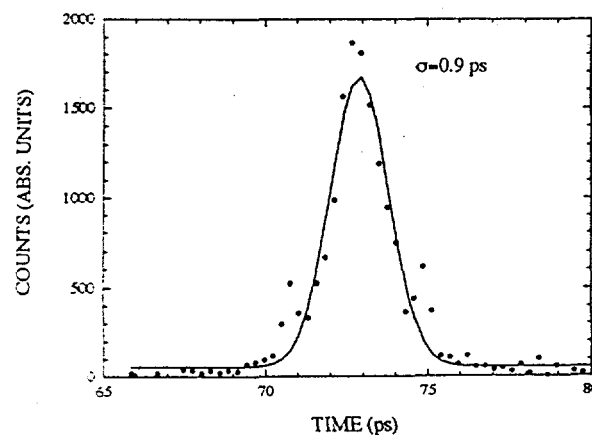
The next case involves data provided courtesy of W. Cieslik of Hamamatsu Photonic Systems on their femtosecond streak camera, FESCA-200 (4). The streak camera was tested with a short pulse ( $\sim 90$  fs (FWHM)) CPM dye laser. The total observed bunch length in Fig. 5 shows two pulses at 180 fs (FWHM) or 80 fs ( $\sigma_{est}$ )



**FIGURE 5.** Streak image obtained with a femtosecond streak camera on a CPM dye laser of 90 ps (FWHM) bunch length. (Data courtesy of Hamamatsu Photonic Systems.)

and a 108 fs pulse. Since these data include the convolution of the bunch length and the streak camera resolution, the resolution is calculated as 160 fs (FWHM) or 68 fs ( $\sigma$ ). The photon statistics are such that the external microchannel plate intensifier appears to be amplifying single photoelectrons which results in intensity fluctuations at the phosphor. A measurement on a linac beam using the Cherenkov mechanism has also been performed indicating a microbunch length of 0.75 ps (FWHM) (8).

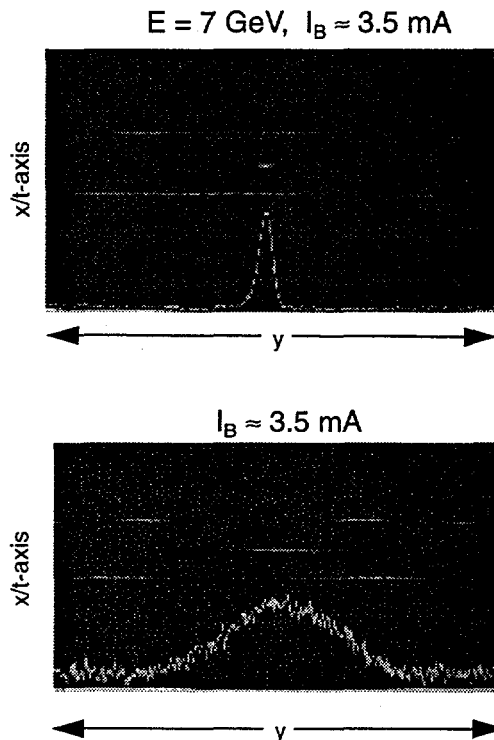
The next cases involve the Hamamatsu C5680 camera which has been used in a series of tests at Argonne National Laboratory. In the first series of experiments, the green component of the Argonne Wakefield Accelerator (AWA) drive laser was measured (9-11). Figure 6 shows the time profile with a Gaussian fit indicating  $\sigma_{tot}$



**FIGURE 6.** Streak image of the green component of the AWA drive laser. Observed bunch length of  $\sigma \sim 0.9$  ps includes the 0.6-ps laser pulse plus the 0.6-ps camera resolution.

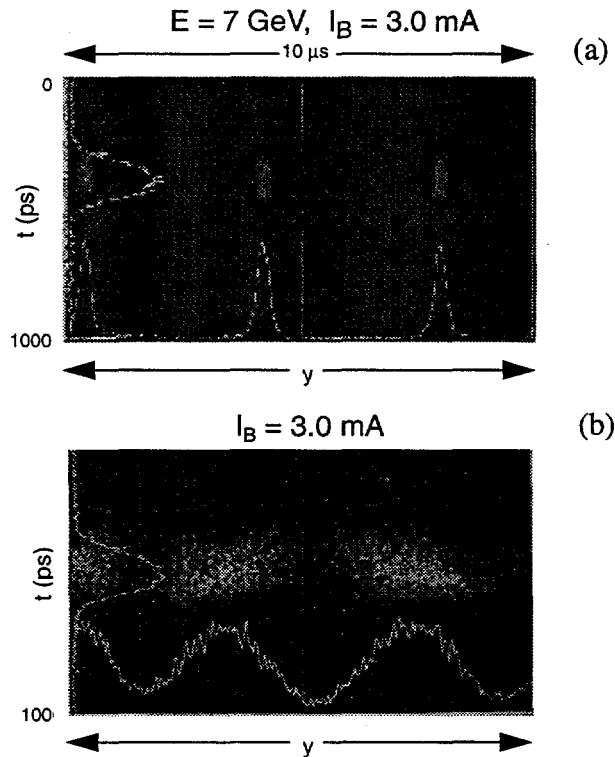
= 0.9 ps. This is the convolved result of about 0.6 ps from the laser bunch and 0.6 ps from the camera resolution. The factory's test data on this tube with the CPM dye laser indicated a resolution of 1.47 ps (FWHM) or 0.62 ps ( $\sigma_{\text{est.}}$ ). These measurements were done with the fast, single-sweep plugin.

The same camera mainframe operates with the synchroscan and dual-sweep plugins as well. The synchroscan unit is tuned at 117.3 MHz, one-third of the 351.9-MHz storage ring rf frequency and equal to the twelfth harmonic of the APS accumulator ring. In the following figures, the identification of the fast head-tail instability at single bunch currents over 1 mA in the APS storage ring is illustrated. In physical space the streak camera is oriented as in Fig. 3, the fast axis is up-down. However, in our transport system from the dipole source point, because we were interested in measuring the fast head-tail vertical instability, the transverse image was rotated 90° before it reached the streak camera slit. The upper part of Fig. 7 shows in focus mode the stable mode with y information on the horizontal axis in the image. The 40- $\mu\text{m}$ -tall slit then samples the image but retains y-profile information. At 3.5 mA, the instability was induced by reducing the sextupole power supply currents and thus the chromaticity values. The lower figure shows an almost 10 times larger y-profile in this condition. The limiting size on the x/t axis is about 5 channels (FWHM), and the range 3 vertical deflection speed gives an effective resolution of about 10 ps (FWHM).



**FIGURE 7.** Focus mode images of the APS storage ring beam showing the beam stable (upper) and unstable (lower) to a vertical fast head-tail instability.

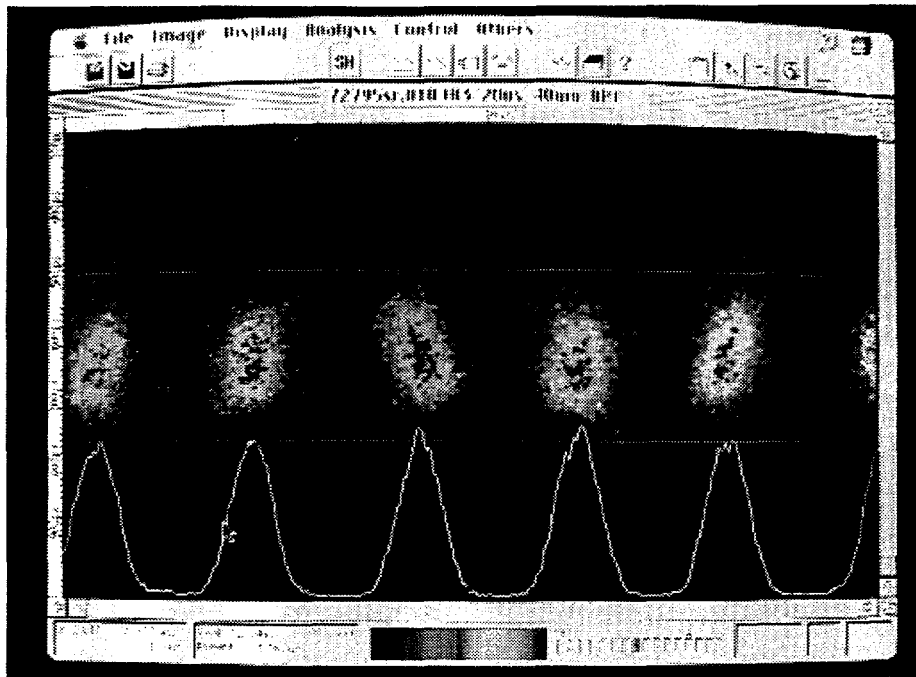
In Fig. 8, the dual sweep feature is used with a 1000-ps span and 10-ps resolution on the vertical axis of the scene and with a 10- $\mu$ s span on the horizontal axis. The "stable" bunch length is  $\Delta t \sim 102$  ps (FWHM). (Keep in mind that R1 is almost an order of magnitude faster sweep than the selected R3.) Figure 8a's streak scene is



**FIGURE 8.** Dual sweep streak images of the APS storage ring beam showing the time-resolved y-profile of the beam in the stable (a) and unstable (b) conditions. Significant y-profile broadening has occurred, and the head-tail tilt on the y-t axis is also visible.

a match to conditions in the upper section of Fig. 7. In Fig. 8b, the projected profiles on the y axis (each turn of the beam takes  $3.68 \mu\text{s}$ ) are about five times larger, and the y-t tilt has rotated visibly in only two turns. The cycle seems to be about three turns which is more evident in Fig. 9 where a  $20\text{-}\mu\text{s}$  slow time axis coverage allows six turns to be displayed. The degree of instability is not as severe as in Fig. 8b.

Another application involved the tracking of the booster synchrotron bunch length during ramping from 0.4 GeV to 7 GeV over 220 ms. In this case, the slowest range (4) was used so the "fast" axis covers 1.5 ns while the horizontal axis covers 100 ms as shown in Fig. 10. The single-bunch turn time is  $1.2 \mu\text{s}$  so the individual turns are not being resolved in this figure. The significant increase in bunch length about 40 ms into the range is apparent in Fig. 10a. One possible interpretation is that a beam loading effect in the rf cavities was occurring. Adjusting the rf cavities in Fig. 10b seemed to compensate for the initial beam loading problems, and the



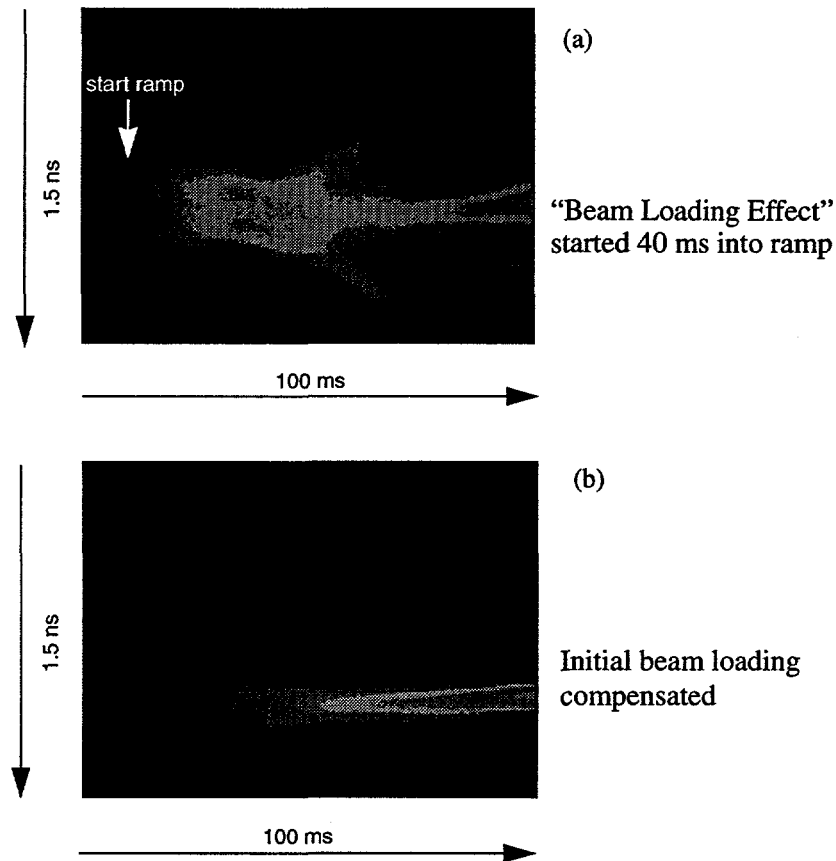
**FIGURE 9.** Fast head-tail vertical instability displayed on a 20- $\mu$ s slow range with the rotation of the y-t tilt changing turn by turn.

image shows the damping as time goes to the right and the relative phase moves upward. Also note the shift in phase on the vertical axis for the center of the images in the two figures. Again, the synchroscan unit is still locked to 117.3 MHz, but the ramp rate in the tube is running at its slowest value.

## RELATED APPLICATIONS

It seems appropriate to note that some of the envisioned injectors for the microbunch beams use a PEI. The drive laser itself can be monitored with the same streak camera. One of our classic examples from the Los Alamos FEL Program involves the observation of shot-to-shot phase jitter in the drive laser. This was directly correlated with the energy jitter of the accelerated electron beam since the photoelectrons would be released at different times in the rf phase (2). This is shown in Fig. 11. The energy shift was about 0.1% per picosecond of phase change. Figure 12 shows the drive laser phase stability improvement (factor of six) when the phase stabilizer was added to the laser. One could anticipate that even better care will be needed for the shorter bunches.

The other potential application is to the SASE or FEL photon beam itself, depending on the wavelength regime. For the purposes of this work, it is noted that some x-ray streak tubes with single-sweep capability have about 0.8 ps ( $\sigma_{est.}$ )



**FIGURE 10.** Dual-sweep streak images of the APS booster synchrotron beam bunch length during the ramping cycle. The significant increase in bunch length about 40 ms into the ramp (a) is compensated in the lower image (b).

resolution. The dual-sweep capability might also be considered for XUV and soft-x-ray applications although the tube geometry constraints indicate  $\sigma_{\text{res}} \sim 1.5\text{-}2.0$  ps then. We have begun tests on a Hamamatsu x-ray tube that is compatible with the synchroscan and dual-sweep plugins of the UV-visible tube (11).

In addition to providing x or y profile information within the microbunch, the axis could be actually converted to wavelength in some cases, such as on a UV-visible FEL or an x-ray FEL sometime in the future. Then the wavelength might be tracked within a micropulse as reported previously (2).

## SUMMARY

In summary, it is evident that time-domain diagnostics could play a critical role in the development of microbunch beams or sources in the coming years. Estimated resolution of  $<70$  fs ( $\sigma$ ) with the power of tracking a transverse profile as well could

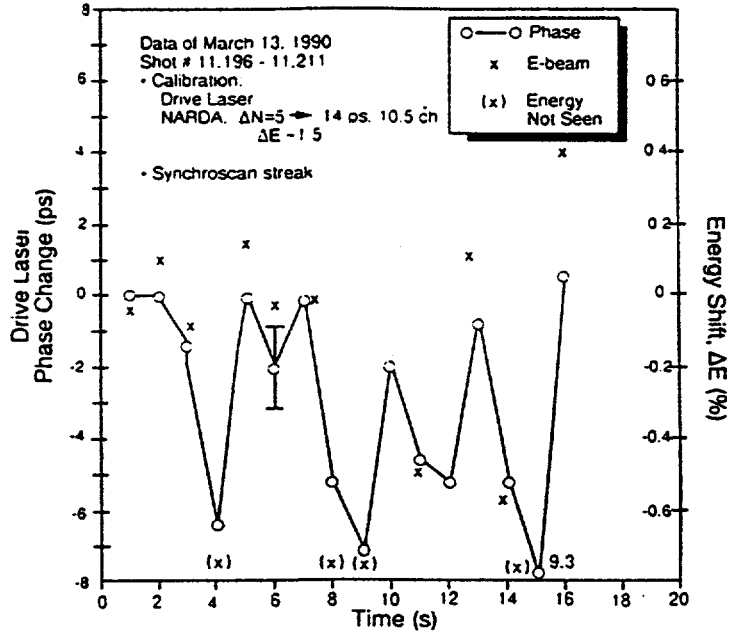


FIGURE 11. Comparisons of drive laser phase jitter shot-to-shot and the observed electron beam energy value in the Los Alamos FEL accelerator

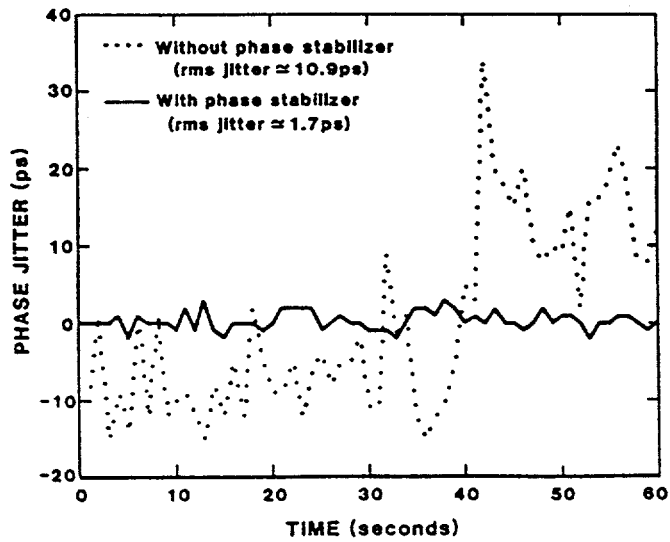


FIGURE 12. Comparison of drive laser phase stability with and without the phase stabilizer circuits active. The rms jitter dropped from about 10.9 ps to 1.7 ps.

be a significant tool. In addition, a trade on resolution ( $<600$  fs ( $\sigma$ )) to get dual-sweep capability may also be valuable in diagnosing the dynamics of linac pulse trains or storage-ring-driven devices, in particular.

## ACKNOWLEDGEMENTS

The author acknowledges Bruce Carlsten (Los Alamos National Laboratory) for providing updated information about the rf deflector; William Cieslik and Masanobu Fujiwara (Hamamatsu Photonic Systems) for providing the 200-fs image data; and Bingxin Yang (Argonne National Laboratory) for his collaboration in the streak camera experiments at Argonne.

## REFERENCES

1. Lumpkin, A. H. and Feldman, D. W., *NIM in Physics Research*, **A259**, 1987, pp. 13–18.
2. Lumpkin, A. H., "Advanced Time-Resolved Imaging Techniques for Electron Beam Characterizations," *AIP Conference Proceedings*, **229**, 1990, pp. 151–179 and reference therein.
3. Lumpkin, A. H., et al., *IEEE Trans. Nucl. Sci.* **NS-30**, 1983, pp. 3139.
4. Takahashi, A., et al., "A New Femtosecond Streak Camera," *SPIE Proceedings*, **2002**, 1993, pp. 22–30.
5. Stein, W. E. and Sheffield, R. L., *NIM in Physics Research*, **A250**, 1986, pp. 12–18.
6. Carlsten, B. E., (private communication Sept. 1995). Also these proceedings.
7. Lumpkin, A. H. and Wilke, M. D., *NIM in Physics Research*, **A331**, 1993, pp. 781–785.
8. Cieslik, W., Hamamatsu Photonic Systems, FESCA-200 Data Sheet, Oct. 1994.
9. Schoessow, P., et al., *Proceedings of the 1993 PAC*, Washington, DC, 1993, pp. 2596–2598.
10. Gai, W., et al., "The AWA Laser System and Its Laser Pulse Shaper," *Proceedings of 1993 PAC*, Washington, DC, 1993), pp. 3050–3052.
11. Lumpkin, A. H., et al., "Initial Tests of the Dual-Sweep Streak Camera System Planned for APS Particle-Beam Diagnostics," *Proceedings of the 1995 PAC*, Dallas, TX, 1995, to be published.